Journal of Applied Physics ARTICLE scitation.org/journal/jap

Exchange current density model for the contact-determined current-voltage behavior of solar cells

Cite as: J. Appl. Phys. **125**, 225302 (2019); doi: 10.1063/1.5090519
Submitted: 28 January 2019 · Accepted: 21 May 2019 ·
Published Online: 11 June 2019

Ellis T. Roe,[1] Kira E. Egelhofer,[2] and Mark C. Lonergan[2,a)]

AFFILIATIONS

[1]Department of Physics, University of Oregon, Eugene, Oregon 97403, USA
[2]Department of Chemistry and Biochemistry, University of Oregon, Eugene, Oregon 97403, USA

[a)]**Electronic mail:** lonergan@uoregon.edu

ABSTRACT

An analytic expression for the current–voltage [$J(V)$] behavior of a solar cell as limited by equilibrium exchange current densities of both carriers at both contacts is derived. The partial currents at both contacts to a generic semiconductor absorber are assumed to be linearly proportional to the excess carrier concentration at the interface with the contacts (e.g., as with Schottky-like contacts). The assumption that the quasi-Fermi levels in the absorber are approximately flat leads to an algebraic solution for the applied voltage as a function of current, which is inverted to obtain the analytic $J(V)$ curve. The $J(V)$ curve reveals distinct behavior associated with electrons and holes, separately, and allows for the determination of all critical performance parameters. In particular, it demonstrates how the characteristic features of the $J(V)$ curve depend on the relative rate at which a particular carrier (electron or hole) is collected at one contact vs the other, rather than the relative rate of electron vs hole collection at a single contact. Furthermore, the model provides a unified explanation of how majority carrier extraction limitations cause nonideal $J(V)$ behaviors such as S-shaped curves and dark/light crossover (i.e., failure of superposition). The efficacy and limitations of the model when applied to Schottky-type and doped semiconductor contacts are discussed. The work serves as a theoretical guide to scientists studying solar cells that are thought to be primarily limited by their contacts.

I. INTRODUCTION

A solar cell, at its most basic level, must consist of an absorber material and two contacts on either end. The limiting current–voltage [$J(V)$] characteristics of solar cells based on the properties of the absorber are well understood.[1–5] The Shockley–Queisser (S-Q) limit[1] is a mathematical determination of the $J(V)$, and hence the efficiency, of a solar cell as limited by the temperature and bandgap of the absorber. In order to derive this limiting efficiency, S-Q assumed that the quasi-Fermi-level splitting in the absorber was equal to the voltage across the device. This is not always the case, however, because the contacts to the absorber must be able to support this voltage by selectively allowing electrons to flow out one end of the device and holes out of the other.[6] A difference between the quasi-Fermi-level splitting in the bulk of a solar cell and the applied voltage is thus related to the rate at which both contacts are able to extract electrons and holes. While the $J(V)$ behavior of a solar cell as determined by bulk recombination processes in the absorber has been calculated in detail, the $J(V)$ characteristics of solar cells as limited by their contacts are less well understood.

In this work, we will calculate an analytic $J(V)$ curve as determined by all "four" rates that dictate electron and hole extraction at "each" contact. Our approach provides both quantitative and intuitive understanding of how a range of contacts can determine solar cell performance. Specifically, our model provides algebraic expressions for critical voltage values that characterize nonideal behavior, such as the inflection point of the S-shaped curve and the voltage at which the light and dark $J(V)$ curves cross each other, in addition to all the standard solar cell performance parameters. Critically, the model adds another potential path to solar cell improvement in the case of nonideal $J(V)$ behavior: it shows that in cases where current rollover is affecting the fill factor of a device, the efficiency can be improved by increasing the extraction rate of the relevant carrier "and/or" by reducing the leakage rate of said

carrier at the "opposite" contact. The model is limited by the extent to which the layer(s) that make up the contacts can be effectively modeled by setting the boundary partial currents proportional to the product of the excess carrier density times a voltage independent constant. We call this boundary condition [see Eq. (6) below] "ideal diode like" in that it is a rate equation describing the net transfer of a given species that has an upper bound in one direction but not the other.

The dependence of solar cell performance on contacts has long been recognized; development of selective contacts for everything from silicon to organics and perovskites has been extensive.[7–14] Theoretical understanding of the mechanisms by which contacts can limit or improve device performance is, however, incomplete. Much of the recent literature, as discussed below, has focused on a contact's ability to either extract its intended carrier or reject the "wrong" carrier. Of course, both contacts in a device must extract their intended carrier "and" reject the wrong carrier to some extent in order for a solar cell to generate power, so a complete understanding of the contacts' limitations on a solar cell should consider all four of these processes.

Throughout this text, we will refer to the collection of the "intended" carrier at a contact as the majority process for that contact and to the associated carrier as the majority carrier. Accordingly, the term minority is used for the "wrong" process/carrier at a contact. Note that we will use the term "bulk majority/minority carrier" explicitly when referring instead to the traditional definition based on the doping of the semiconductor.

The notion that a solar cell's performance can be limited by a contact's ability to extract its majority carrier is intuitive. Indeed, numerous studies have explored how this can limit the open-circuit voltage (V_{oc}) of a device.[15–20] Wagenpfahl *et al.* calculated an analytic expression for the V_{oc} of a solar cell due to an electric field associated with the buildup of majority carriers at a contact that is caused by the reduction of the charge transfer velocity of majority carriers.[16] Simulated $J(V)$ also suggested that a reduced charge transfer velocity of majority carriers at a contact can be the cause of so-called S-shaped curves that can ruin the fill factor. This notion was confirmed by Sandberg *et al.* whose simulations also showed S-shaped curves being affected by the injection barrier, carrier mobilities, and trap densities at the interface.[17] Niemegeers and Burgelman used a back-to-back diode equivalent circuit to model the current "rollover" effect (analogous to S-shaped curves) in CdTe solar cells.[15] The saturation current of the back diode, quantifying the collection of majority carrier holes, is limited by the work function alignment of the metal used for the back contact; this was shown to determine the current value at which the $J(V)$ curve rolls over in forward bias, thus affecting the fill factor of the device. Barriers to the extraction of majority carriers have also been linked to nonideal $J(V)$ behavior in silicon-based devices. Chavali *et al.*[21] developed a numerical model to explain the nonideal S-shaped behavior found in $J(V)$ measurements of a-Si/c-Si devices seen by Das *et al.*[22] They found that the "knee" in such nonideal $J(V)$ curves occurs when the current at the relevant interface goes from being dominated by one carrier to the other. For higher "knee" voltages, the S-shaped curve is avoided, and the *FF* is improved.

It is equally intuitive that the failure of a contact to reject the wrong carrier, or minority carrier, leads to unwanted surface recombination and, hence, reduced efficiency. Mora-Sero and Bisquert considered a "sandwich" model (i.e., an absorber sandwiched by two different contacts) using one ideal contact paired with a contact whose selectivity is reduced by allowing electrons to escape depending on ρ, the resistivity to minority carrier flow at the contact.[23] They calculated a $J(V)$ curve whose V_{oc} and J_{sc} are strongly affected by ρ. Sandberg *et al.* also considered a sandwich-type solar cell architecture and derived analytic expressions for the V_{oc} in various regimes delineated by ohmic vs nonohmic contacts.[19] For a single nonohmic contact paired with an ohmic contact, regimes dominated by diffusion-limited surface recombination and interface-kinetics-limited surface recombination were considered. They calculated an effective diffusion velocity parameter following Crowell and Sze[24] that, compared to the charge transfer velocity of minority carriers, can be used to determine whether kinetics or diffusion determine recombination rates at V_{oc}.

Brendel and Peibst defined selectivity as the ratio of the minority to majority carrier resistivity of an interface and modeled $J(V)$ behavior with a diode characterized by the minority-carrier resistivity in series with a resistor determined by the majority carrier resistivity.[18] This allowed them to determine the optimum contact area for various types of silicon solar cells based on the selectivity (i.e., resistivity) ratio of the contact. This model hints at the potential interplay between both "majority" and "minority" processes at a contact determining device performance, a concept touched on by others.[16,25] However, none of the above models consider all four processes independently.

For additional context, it is instructive to take a step back from these focused studies and consider a simpler, more general model. Perhaps, the simplest theoretical model of contact-limited $J(V)$ behavior is a parallel combination of a diode governed by the ideal diode equation and a current source whose current value is J_L (i.e., the light current). The $J(V)$ curve for such a device obeys

$$J(V) = J_0(e^{V/V_T} - 1) - J_L. \tag{1}$$

Here, V_T is the thermal voltage, i.e., k_BT/q, where k_B is the Boltzmann constant, T is the temperature, q is the electron charge, and J_0 is the equilibrium exchange current density or saturation current density. This is effectively the same equation as that derived in the S-Q limit, except as we will see, J_0 in this case is determined entirely by the contact(s) and not by radiative recombination in the bulk. The maximum power (density) of a device obeying Eq. (1) is determined by the balance of J_0 and J_L, given by

$$P_{max} = J(V_{max}) \times V_{max}, \tag{2}$$

where

$$V_{max} = V_T\left(W\left[e\left(1 + \frac{J_L}{J_0}\right)\right]\right) \tag{3}$$

and W is the Lambert W function. As is commonly understood, the ratio of J_L to J_0 determines the efficiency, thus minimizing J_0 is critical to maximizing the device efficiency.

The origin of J_0 depends on which simple diode model we consider. In the case of the Schottky diode, J_0 is determined by the potential barrier for bulk majority carriers at the metal–semiconductor

interface via thermionic emission,

$$J_0 = A^* T^2 e^{-\frac{\phi_b}{qV_T}}, \tag{4}$$

where ϕ_b is the barrier height (i.e., ϕ_b is the energy difference between the band of the bulk majority carrier and the Fermi level at the interface at equilibrium) and A^* is the effective Richardson constant.[26] Note that while one considers the rate of bulk majority carriers that are able to escape the potential barrier at the interface, these carriers are the minority carriers at the interface. In other words, for a typical Schottky diode based on a p-type semiconductor, the Fermi level of the isolated metal used to make the contact is generally located in the top half of the bandgap, meaning that it is effectively an electron-selective contact. J_0 in this case measures the ability of holes to travel over the potential barrier at the interface, where they are considered minority carriers in this work.

Meanwhile, for the Shockley model of a p–n junction, J_0 is calculated by considering the diffusion of minority carriers on either side of the depletion region.[27] Here,

$$J_0 = q\left(\frac{D_p p_{n0}}{L_p} + \frac{D_n n_{p0}}{L_n}\right), \tag{5}$$

where D_p is the diffusion constant for holes, p_{n0} is the equilibrium concentration for holes on the n-type side, and L_p is the hole diffusion length and vice versa for the other term. The origin of this J_0 is, of course, bulk recombination in the quasineutral regions on both sides of the depletion region. However, because typical p–n junctions have good ohmic contacts on both sides, the "interfaces" between the depletion region (in which recombination is neglected) and the quasineutral regions on both sides are the rate-determining interfaces. In this way, the p and n quasineutral regions can be thought of as the contacts to the depletion region. Thus, the two terms in J_0 are determined by the recombination of minority carriers for each contact (i.e., holes on the n-side and electrons on the p-side).

The performance of the simple solar cell model of Eq. (1) is limited in both cases by carriers escaping to the wrong contact. For the Schottky diode, only one J_0 is considered, associated with the rectifying contact. Meanwhile, with the p–n junction, two J_0's are considered; one for each side of the junction resulting in the two terms of Eq. (5). In order to reduce the escape of minority carriers in the ideal Schottky diode, one can either use a metal whose Fermi level is closer to the intended carrier's band or one can introduce a thin insulating layer that reduces the flow of both carriers.[28–30] For the p–n junction, reduction of minority carrier leakage can be achieved by strongly doping the n and p layers. This has already been recognized; the state-of-the-art silicon technology uses highly n and p doped regions as the electron and hole selective contacts, respectively.[30,31]

It is critical to note that in both the Shockley model of the p–n junction and the Schottky diode model, one effectively assumes that the bulk quasi-Fermi-level splitting is equal to the applied voltage. For the p–n junction, this is guaranteed with the assumption of low injection of majority carriers at the edges of the depletion region. With the Schottky diode, one implicitly assumes that the other contact to, for instance, our p-type material is able to perfectly extract holes. In other words, one assumes for both cases that the majority processes at each contact are very fast so that no buildup of that carrier is required at the contact in order to support the current. This assumption is not generally valid, nor can one always assume perfect rejection of minority carriers at a contact; a thorough contact-determined solar cell model must consider the ability of majority carriers to escape "as well as" the ability of minority carriers to escape at "both" contacts.

Recently, we proposed a model for contact-limited solar cells which we used to calculate an analytic expression for the V_{oc} as a function of the four J_0's determined by the two contacts to an intrinsic absorber for both carriers.[32] We found that the nature of V_{oc} depends on the relation between the larger of J_0's at each contact and the light-generated current, J_L. As long as J_0's for both majority processes at the contacts are much larger than the light current, the V_{oc} is equal to the quasi-Fermi-level splitting, and both are determined by contact recombination due to carriers arriving at the wrong contact and recombining. On the other hand, if both the majority J_0's are smaller than the light current, the V_{oc} will be smaller than the quasi-Fermi-level splitting and will depend on all four exchange current densities equally. In this case, the selectivity (i.e., asymmetry) limits the V_{oc}, and in the case of ideal Schottky contacts, the V_{oc} is equal to the difference in work functions of the contacts.

As discussed above, our analysis focuses on the effect of J_0's on the performance of the solar cell, and thus, it is important to note that they are measurable quantities associated with an interface.[33–37] Refer to the supplementary material for a simulated example of how the four J_0's of a solar cell can be measured and used to predict the solar cell's $J(V)$ behavior.

In this text, we use the contact-determined device model from the previous work to derive the full analytic $J(V)$ curve as a function of the light current and the four exchange current densities of the contacts. While V_{oc} is a critical factor for device performance, knowledge of the full $J(V)$ curve is essential to determine the power conversion efficiency, as the fill factor (FF) and short circuit current (J_{sc}) can also be affected by the contacts. Our model can provide a useful theoretical reference, analogous to the ideal diode equation, for solar cells with contacts that can be approximated by the ideal diode like boundary conditions employed.

II. THEORY

The model we employ has been described in detail in our previous work[32] and no new assumptions have been introduced. The essential features will be summarized here.

Our model consists of an intrinsic semiconductor absorber sandwiched by two contacts, denoted α and β contacts (see Fig. 1). Generation of electrons and holes is assumed to be constant throughout the absorber. Unlike at V_{oc}, at arbitrary voltages, carriers can enter the device either by generation or by injection from the contacts. The x-axis runs from the α contact at x^α to the β contact at x^β. Positive current is assigned to holes moving in the positive x-direction, i.e., from left to right. We make the following assumptions:

(1) Electrons (holes) in the conduction (valence) band can be described by an electron (hole) electrochemical potential, or quasi-Fermi level, $\bar{\mu}_n$ ($\bar{\mu}_p$). Here, $\bar{\mu} = \mu + zq\phi$, where μ is the

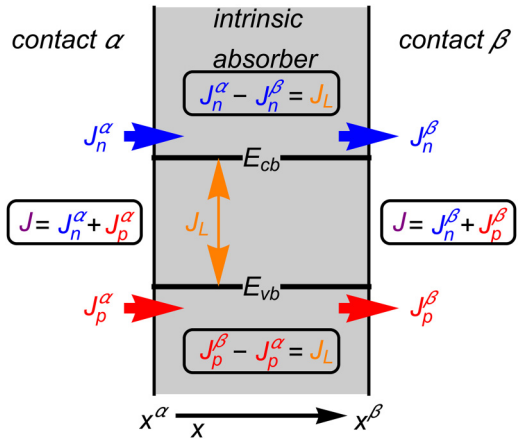

FIG. 1. Depiction of the essential features of our solar cell model consisting of an intrinsic absorber and two contacts. Relations between the four partial currents of each carrier at each contact are highlighted in the black boxes. The partial currents must sum to the total current, J, at both contacts and the difference between the partial currents of the same carrier across the device is equal to J_L.

relevant chemical potential, ϕ is the electrostatic potential, and z is $+1$ for holes and -1 for electrons. This assumption requires that the individual carriers are in equilibrium with their respective bands, i.e., that the carriers are thermalized.

(2) There are no transport limitations in the absorber so that slopes in the quasi-Fermi levels are negligibly small (i.e., $d\bar{\mu}_n/dx \approx d\bar{\mu}_p/dx \approx 0$).

(3) Bulk recombination is negligibly small as compared to contact recombination. Note that this assumption and assumption 2 are implicitly required in both the classic p-n junction and Schottky diode models. We will quantitatively test these assumptions in Sec. IV.

(4) Ideal diode like boundary conditions for the electron and hole partial currents J_n and J_p at each interface are assumed as

$$J_n(x^\alpha) = J_n^\alpha = J_{0n}^\alpha\left(\frac{n(x^\alpha)}{n_0(x^\alpha)} - 1\right), \tag{6a}$$

$$J_p(x^\alpha) = J_p^\alpha = -J_{0p}^\alpha\left(\frac{p(x^\alpha)}{p_0(x^\alpha)} - 1\right), \tag{6b}$$

$$J_n(x^\beta) = J_n^\beta = -J_{0n}^\beta\left(\frac{n(x^\beta)}{n_0(x^\beta)} - 1\right), \tag{6c}$$

$$J_p(x^\beta) = J_p^\beta = J_{0p}^\beta\left(\frac{p(x^\beta)}{p_0(x^\beta)} - 1\right), \tag{6d}$$

where x^α and x^β are the positions of the interfaces for the contacts α and β, respectively, J_{0n} and J_{0p} are (voltage independent) the electron and hole equilibrium exchange current densities, n and p are the electron and hole carrier concentrations, and n_0 and p_0 their equilibrium values.

(5) Equilibrium carrier concentrations obey the law of mass action

$$n_0(x)p_0(x) = n_i^2, \tag{7}$$

where n_i is the intrinsic carrier concentration.

(6) The electric field in the contacts is zero, and both chemical potentials in the contacts, $\mu^{(\beta)}$ and $\mu^{(\alpha)}$, are independent of voltage.

The ideal diode like rate equations that describe the boundary conditions for the partial currents, Eq. (6), are appropriate for the thermionic emission of carriers, as in the Schottky model of the metal–semiconductor interface. While many solar cell archetypes use more complicated architectures, it should be noted that some should follow similar boundary conditions to Eq. (6) in that the partial currents are equal to a voltage independent constant multiplied by the excess carrier density at the contact, where the equilibrium density is set by the Fermi level of the contact, be it a semiconductor or metal. In Sec. IV and the supplementary material, we test our model with the use of doped heterojunction contacts, in addition to simple Schottky metal contacts.

It is important to emphasize that the above assumptions are no more restrictive than the assumptions that S-Q made or even compared to the assumptions used to derive the ideal diode equation. The purpose of this work is to derive the ideal $J(V)$ behavior of a contact-limited device.

Under our assumptions, the continuity equation is easily solved for electrons, giving

$$J_n^\alpha - J_n^\beta = J_L. \tag{8}$$

Here, $J_L = \int_{x^\alpha}^{x^\beta} qG_L(x)dx$, where G_L is the generation rate per unit volume and q is the charge of an electron. Note that we could easily use the corresponding equation for holes instead; they are not independent constraints. Following the previous work,[32] the carrier concentrations at the contacts are constrained by

$$n(x^\alpha)p(x^\alpha) = p(x^\beta)n(x^\beta), \tag{9}$$

where the carrier concentrations are again evaluated at the contacts as in Eq. (6). The sum of electron and hole currents must be independent of position throughout the device in steady state. Evaluated at each contact then,

$$J_n(x^\alpha) + J_p(x^\alpha) = J, \tag{10a}$$

$$J_n(x^\beta) + J_p(x^\beta) = J, \tag{10b}$$

where J is the total current density of the device. Equation (9) can be rewritten in terms of the partial currents at the contacts using Eq. (6). Equations (8), (10a), and (10b) are then used to eliminate all variables except J_n^β.

The voltage difference across the device, V, can be written in terms of the carrier concentrations evaluated at the contacts via

$$V = V_T \ln\frac{n(x^\alpha)n_0(x^\beta)}{n_0(x^\alpha)n(x^\beta)}. \tag{11}$$

In order to derive an expression for $V(J)$, we rewrite V as function of the partial current already solved for (J_n^β, for instance) using Eq. (6), then plug in the solution to J_n^β. Once simplified, this expression for $V(J)$ can be inverted and simplified to produce $J(V)$. The solution is algebraic, and no approximations were used. For brevity, the derivation has been omitted from the text; refer to the supplementary material for a detailed algebraic derivation.

III. RESULTS AND DISCUSSION

The $J(V)$ characteristics of a contact-limited solar cell under our assumptions as derived algebraically in the supplementary material are

$$J(V) = -\left(J_L + j_{0n}^\alpha + j_{0p}^\beta\right) + \frac{J_L + j_{0n}^\alpha + \mathbf{J_{0n}^\beta}}{1 + \frac{\mathbf{J_{0n}^\beta}}{j_{0n}^\alpha} e^{-V/V_T}} + \frac{J_L + j_{0p}^\beta + \mathbf{J_{0p}^\alpha}}{1 + \frac{\mathbf{J_{0p}^\alpha}}{j_{0p}^\beta} e^{-V/V_T}}. \tag{12}$$

Here, we have assumed that for the β contact, the electron J_0 is larger than the hole J_0 and vice versa for the α contact. Thus, we have used j_0 for the smaller, or minority J_0, associated with a contact and $\mathbf{J_0}$ for the larger, or majority J_0. While this assumption is not necessary to calculate performance parameters or even to make a functioning solar cell (see Fig. 3), it is useful in understanding the behavior of the function.

A. Two steps in every curve

It is perhaps easiest to think of Eq. (12) as having three terms. The first term, $-\left(J_L + j_{0n}^\alpha + j_{0p}^\beta\right)$, is voltage independent. This current value is essentially the reverse bias saturation current plus J_L. The other two terms are voltage dependent, but the first depends only on J_L and electron J_0's, while the second depends only on J_L and hole J_0's. The functional forms of both voltage dependent terms are smeared-out step functions, thus, we dub one the "electron step" and the other the "hole step." Therefore, the $J(V)$ curve is, in general, a superposition of two smeared step functions, one associated with the electrons and the other associated with holes, offset by $-\left(J_L + j_{0n}^\alpha + j_{0p}^\beta\right)$. We have provided a physical explanation of the critical features of the $J(V)$ behavior in the supplementary material.

Note that, in practice, the leveling off of the second step is unlikely to be observed for the vast majority of solar cells. This is because there is usually at least one contact in a solar cell that is really good at extracting its intended carrier, and thus, the current at which the $J(V)$ curve levels off is unlikely to be measured. Furthermore, for real devices, bulk recombination will always kick in eventually in forward bias. This allows for the difference between partial currents across the device to be unbounded, allowing the current to go to infinity like a normal diode. This will occur in place of the second step whenever J_0 associated with bulk recombination processes is larger than the smallest j_0. Regardless, the physical origin of the second step is useful in understanding the relative importance of electron and holes processes in the operation of a solar cell.

The electron and hole steps are characterized by their height and the voltage at which they are centered. The height of the electron step is equal to $J_L + \mathbf{J_{0n}^\beta} + j_{0n}^\alpha$, and the height of the hole step is, analogously, $J_L + \mathbf{J_{0p}^\alpha} + j_{0p}^\beta$. The inflection point, or "center" of the step (i.e., when the current is exactly halfway between the lower and upper values of the step), is easily calculated for both steps. This "step" voltage is

$$V_{s,n} = V_T \ln\left(\frac{\mathbf{J_{0n}^\beta}}{j_{0n}^\alpha}\right) = V_T \ln(S_n), \tag{13a}$$

$$V_{s,p} = V_T \ln\left(\frac{\mathbf{J_{0p}^\alpha}}{j_{0p}^\beta}\right) = V_T \ln(S_p), \tag{13b}$$

for electrons and holes, respectively. Here, we have introduced the electron and hole "carrier" selectivities as

$$S_n = \frac{\mathbf{J_{0n}^\beta}}{j_{0n}^\alpha}, \tag{14a}$$

$$S_p = \frac{\mathbf{J_{0p}^\alpha}}{j_{0p}^\beta}, \tag{14b}$$

respectively. Note that the carrier selectivity for both electrons and holes involves J_0's from both contacts. Also note that this definition could just as easily be written as a ratio of surface recombination velocities multiplied by the ratio of equilibrium carrier densities for a given carrier at each contact. In the case of the Schottky contact, for example, the carrier selectivity is controlled both by the ratio of the Richardson constants on both sides, as well as the equilibrium carrier densities, as set by the barrier heights. The carrier selectivity is distinct from the notion of "contact" selectivity, which was defined in our previous work as the ratio of the two J_0's of a single contact. A critical result of our theory then is that the $J(V)$ characteristics of the contact-determined solar cell depend on the "carrier" selectivities and not on the selectivity of an individual contact.

Equation (12) provides a unified treatment of nonideal solar cell phenomena such as dark/light crossover (i.e., failure of current superposition)[38,39] and S-shaped curves.[21] For instance, it is immediately evident from Eq. (12) that the $J(V)$ curve cannot be written, in general, as $J_{dark}(V) + J_{light}$, where J_{light} is voltage independent. In fact, the voltage at which the current crossover occurs can easily be calculated by setting Eq. (12) equal to itself with and without J_L and solving for V. The solution is given by

$$V_{cross} = V_T \ln\left(\frac{J_{0n}^\beta J_{0p}^\alpha}{J_{0n}^\alpha J_{0p}^\beta}\right) = V_T \ln(S_n S_p). \tag{15}$$

This equation predicts that there is "always" dark/light crossover in "every" contact-limited solar cell. However, if the product of the selectivities is large enough, one may not be able to measure it because the current is likely to become strongly affected by series resistance far into forward bias. Not only does crossover always happen in principle, the $J(V)$ is always S-shaped in principle. Both

phenomena are natural consequences of including the limitations due to majority carrier exctraction for both carriers in the model. However, they only become relevant to the power quadrant when J_L is larger than $\mathbf{J_0}$'s. This is discussed in more detail below.

B. Sample $J(V)$ curves

Figure 2 is an example $J(V)$ curve produced from Eq. (12), demonstrating the key features of the function. In reverse bias ($V < 0$), the current is approximately J_L, given that j_0's are much smaller than J_L. We can tell that j_0's are small relative to J_L and the $\mathbf{J_0}$'s just by glancing at the curve; they must be small in order for there to be an appreciable photovoltaic effect. In this example, the two steps are well separated in voltage. The first step (i.e., the step that occurs at smaller forward bias, colored blue in Fig. 2) is associated entirely with electron J_0's in this case. We can immediately tell from where the electron step ends (at $+10\,\mathrm{mA\,cm^{-2}}$) that $\mathbf{J}^{\beta}_{\mathbf{0n}} = 10\,\mathrm{mA\,cm^{-2}}$ because the height of the electron step is approximately equal to $J_L + \mathbf{J}^{\beta}_{\mathbf{0n}}$. Since the two steps are well separated in voltage, we can use the location of the center of the electron step at $\sim 420\,\mathrm{mV}$ (labeled V_n in Fig. 2) to calculate the value of j^{α}_{0n} from Eq. (13a). Given a temperature of 300 K for Fig. 2, and that $\mathbf{J}^{\beta}_{\mathbf{0n}} = 10\,\mathrm{mA\,cm^{-2}}$ as discovered above, $j^{\alpha}_{0n} \approx 10^{-6}\,\mathrm{mA\,cm^{-2}}$. In this case, the value for j^{α}_{0n} could also be determined or confirmed from the saturation current of a dark $J(V)$ measurement, since j^{β}_{0p} is much smaller than j^{α}_{0n}. The hole step, colored red in Fig. 2, occurs entirely outside of the power quadrant and, therefore, does not limit the efficiency of the device.

In the case of Fig. 2, the solar cell is limited by the "electron selectivity." Therefore, any increase in that ratio, either from decreasing j^{α}_{0n} or by increasing $\mathbf{J}^{\beta}_{\mathbf{0n}}$ will improve the efficiency of the device while changing the hole-associated J_0's will have no appreciable effect on the efficiency of the device. This knowledge is useful because it tells us that an appropriate improvement in "either" contact will increase device performance. Practically speaking, this means we might be able to improve the device efficiency with a thin insulating layer inserted at the α contact. Although this would likely decrease $\mathbf{J}^{\alpha}_{\mathbf{0p}}$, that does not affect the power quadrant, while reducing j^{α}_{0n} would improve the electron selectivity by reducing electron leakage.

Another consequence of the importance of carrier selectivity is that it is entirely possible to create a functional solar cell where both contacts are electron-selective (or both are hole selective) as long as both carriers have at least "some" preference for opposite contacts. Here, by electron-selective contact, we mean a contact whose electron J_0 is larger than its hole J_0 and vice versa for a hole selective contact. Figure 3 is an example of a $J(V)$ curve for a solar cell with two electron-selective contacts, yet there is still an appreciable photovoltaic effect. Despite the fact that both contacts are electron-selective, the holes still prefer the α compared to the β contact and vice versa for electrons because one contact is "much" more selective than the other. Note that while it is possible to create a functioning solar cell with two contacts of the same selectivity type or even if one of the two contacts is not selective, it is "not" possible to create a functioning solar cell if "neither" contact is selective. The requirement to achieve an appreciable photovoltaic effect in all cases is simply that the contacts encourage electrons to go to one contact and holes to the other contact. In other words, if the electrons prefer contact β due to it having a larger electron J_0 than contact α, the opposite must be true for holes.

C. Low and high injection

In principle, all contact-determined $J(V)$ curves produced by Eq. (12) are a simple superposition of the two steps centered at the step voltages for each carrier. However, because the current offset from zero (i.e., the current in reverse bias) is approximately equal to J_L and because only the power quadrant determines device performance, it is important to consider the size of the steps relative to the light current. According to Eq. (12), each step has a minimum height of J_L when the $\mathbf{J_0}$ associated with the step is small compared to J_L. Conversely, if the $\mathbf{J_0}$ associated with a step is much larger

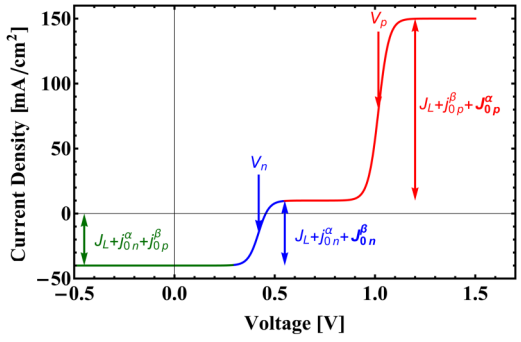

FIG. 2. A sample current–voltage curve produced by Eq. (12) using $J_L = 40$, $\mathbf{J}^{\beta}_{\mathbf{0n}} = 10$, $j^{\alpha}_{0n} = 10^{-6}$, $\mathbf{J}^{\alpha}_{\mathbf{0p}} = 100$, $j^{\beta}_{0p} = 10^{-15}\,\mathrm{mA\,cm^{-2}}$. The colors are used as an aid to understanding the function. In green, the current is fixed at approximately J_L. The blue section highlights the first step, whose location is determined, in this case, by electron J_0's. The red section highlights the second step, in this case entirely determined by hole J_0's.

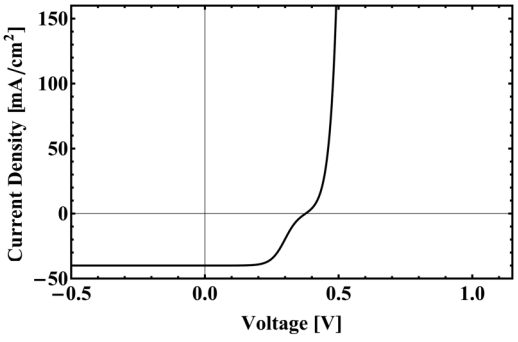

FIG. 3. An example of a $J(V)$ curve produced by Eq. (12) in which the electron J_0's of each contact are larger than the hole J_0's, meaning both contacts are electron-selective. Parameter values are $J_L = 40$, $J^{\beta}_{0n} = 10^{6}$, $J^{\alpha}_{0n} = 10^{-6}$, $J^{\alpha}_{0p} = 10^{-8}$, $J^{\beta}_{0p} = 10^{-13}\,\mathrm{mA\,cm^{-2}}$. Note that we have not used the $\mathbf{J_0}$, j_0 convention because the assumption that both contacts have the opposite selectivity is not valid in this case.

than J_L, the height of that step is approximately equal to that $\mathbf{J_0}$. These two limits naturally suggest two regimes that delineate distinct behavior for each carrier. A carrier is in high injection when the equilibrium exchange current density for the carrier's majority J_0 is much smaller than J_L, i.e., electrons are in high injection if $J_L \gg \mathbf{J}_{\mathbf{0n}}^{\beta}$. The low injection limit applies to a carrier if the $\mathbf{J_0}$ of the carrier is much larger than J_L. As we have shown previously,[32] these regimes correspond to different orders of recombination at the contacts; the high injection regime is associated with second order recombination while the low injection regime indicates the presence of quasi-first-order recombination.

The motivation to separate these two regimes can be taken from Eq. (6). The majority process is a significant limitation to device performance when a large excess of majority carriers is needed to provide a partial current on the order of J_L, which is necessary for any solar cell. In other words, the "high injection" limit is that where the majority carrier density at a contact interface must be much larger than the equilibrium density as set by the contact in order to generate J_L of partial current. The "low injection" limit meanwhile implies that only a very small excess of majority carriers at the contact is required to produce J_L. This naturally leads to the direct comparison of J_L to the $\mathbf{J_0}$ for each carrier. The difference between our definition of low and high injection and the usual definition is the density to which we compare the majority carrier density; in usual device physics, one compares to the dopant density, whereas here we compare to the equilibrium density as set by the contact. Note that we could easily define such a limit for the minority carriers as well; however, one cannot produce an appreciable photovoltaic effect if $j_0 > J_L$, therefore, minority carriers are always in "high injection" for all practical solar cells.

Figures 4(a) and 4(b) display $J(V)$ curves where the first, or limiting step, is in low and high injection, respectively [refer to the supplementary material for log plots of the dark $J(V)$ curves]. They reproduce the approximate performance parameters and shape from Figs. 5(a) and 6(a) from Das *et al.*,[22] respectively, where various passivating amorphous silicon layers were used as selective contacts to either side of a crystalline silicon absorber. For the low-injection case, the $J(V)$ curve will always look qualitatively similar to Fig. 4(a) on the scale of J_L. That is, there will only be one visible step, and the current will not level off on the scale of J_L. The $J(V)$ curve is still S-shaped, but the S will not appear on the scale of J_L, meaning it will be irrelevant to the power quadrant, thus, the superposition principle applies in the power quadrant. This is perhaps the simplest case, and it can be shown (see Sec. III D 1) that the efficiency is solely dependent on the limiting j_0. The only way to improve such a device is to reduce the leakage rate of minority carriers and because holes are the limiting carriers in this case, this means decreasing j_{0p}^{β}.

In contrast, the $J(V)$ curve can also look like Fig. 4(b) where the superposition principle clearly fails, producing an S-shaped curve in the power quadrant because the limiting carriers (holes, in this case) are in high injection. The step for a carrier that is in high injection always ends at $J \approx 0$ (except when the steps occur at the same voltage), leading to a less-than-ideal fill factor. While electron J_0's can effect the V_{oc} in this case, they do not have a significant effect on the power quadrant and hence the efficiency as they are not the limiting carrier. As with Fig. 2, our model states that one

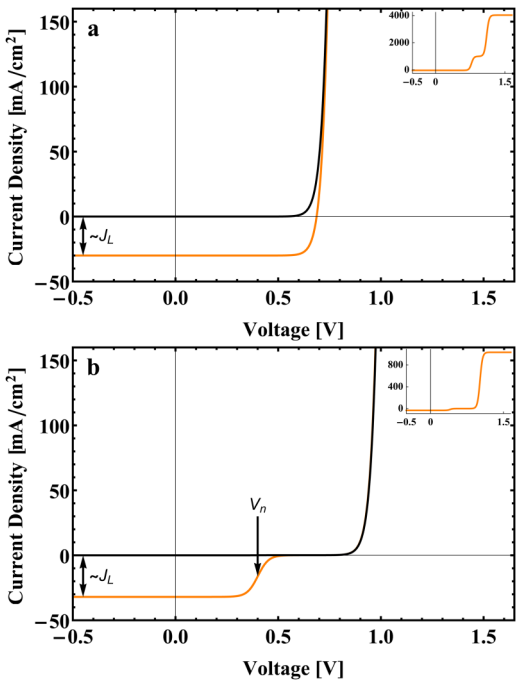

FIG. 4. (a) Dark (black) and light (orange) $J(V)$ curves produced from Eq. (12) using $J_L = 30$, $\mathbf{J}_{\mathbf{0n}}^{\beta} = 3 \times 10^3$, $j_{0n}^{\alpha} = 10^{-15}$, $\mathbf{J}_{\mathbf{0p}}^{\alpha} = 10^3$, $j_{0p}^{\beta} = 10^{-10}$ mA cm^{-2}. The limiting carriers are in this case holes, which are in low injection. The inset shows the light $J(V)$ curve on a current scale sufficient to observe the biggest step. (b) $J(V)$ curves produced using $J_L = 32$, $\mathbf{J}_{\mathbf{0n}}^{\beta} = 10^3$, $j_{0n}^{\alpha} = 10^{-14}$, $\mathbf{J}_{\mathbf{0p}}^{\alpha} = 10^{-1}$, $j_{0p}^{\beta} = 2 \times 10^{-8}$ mA cm^{-2}. The limiting carriers are again holes which are now in high injection. The electrons are in low injection. The inset again depicts the light $J(V)$ curve on a current scale sufficient to see both steps in their entirety.

could improve the device efficiency "both" by increasing the limiting $\mathbf{J_0}$ (in this case, $\mathbf{J}_{\mathbf{0p}}^{\alpha}$) and by decreasing the limiting j_0 (in this case, j_{0p}^{β}). This might be useful, if for instance, it is not clear how to improve the hole "collection" of contact α. This is particularly insightful because, for instance, the thin-film/CdTe literature has frequently correlated current rollover to limited built-in potential, caused by an undesired barrier at the back contact.[15,39,40] Our explanation is consistent with this because the back barrier is what determines J_0's for that contact, but we also show that improvements to the opposite contact would also be beneficial to performance. If instead, one "was" able to increase $\mathbf{J}_{\mathbf{0p}}^{\alpha}$, an improvement of 2.5 orders of magnitude would be useful after which reducing j_{0p}^{β} would be the only way to improve efficiency.

The above discussion relied heavily on the term "limiting carrier/process," and thus, it is important to be precise about their definition. One might assume that the carrier with the smallest step voltage [Eq. (13)] must be the limiting carrier, but this is only appropriate if both carriers are in high injection. If a carrier is in low injection, then the step voltage is not relevant to the power quadrant because the current at the step voltage will be well above zero (i.e., outside the power quadrant). In this case, it is the ratio of

J_L (instead of $\mathbf{J_0}$) to j_0 that must be considered. We, therefore, define the critical voltages for each carrier as

$$V_{c,n} = V_T \ln\left(\mathrm{Min}\left[\frac{\mathbf{J_{0n}^{\beta}}}{j_{0n}^{\alpha}}, \frac{J_L}{j_{0n}^{\alpha}}\right]\right), \tag{16a}$$

$$V_{c,p} = V_T \ln\left(\mathrm{Min}\left[\frac{\mathbf{J_{0p}^{\alpha}}}{j_{0p}^{\beta}}, \frac{J_L}{j_{0p}^{\beta}}\right]\right). \tag{16b}$$

The carrier with the smallest critical voltage is the limiting carrier. If the critical voltages are within a few kT/q of each other, both carriers will limit the device.

Note that if both contacts are ideal Schottky contacts, the carrier selectivities will be equal (see the supplementary material). However, the critical voltages of each carrier may not be equal in that case, depending on the work functions of the metals. Since many semiconductor–metal interfaces do not behave as ideal Schottky contacts, and since many solar cells use interfacial layers and/or doped semiconductors (as opposed to just a metal) as contacts to the absorber, one would expect that in practice, the carrier selectivities of electrons and holes will not generally be identical.

D. Solar cell performance parameters

Equation (12) can be used to calculate the critical performance parameters of a solar cell. J_{sc} can be determined, in general, by setting the voltage to zero and simplifying the expression (see the supplementary material) leading to

$$J_{sc} = J_L\left(\frac{1}{1+S_p} - \frac{1}{1+1/S_n}\right). \tag{17}$$

According to Eq. (17), the maximum value of J_{sc} is J_L. This occurs when both carrier selectivities go to infinity. The value of J_{sc} is linearly dependent on J_L, and thus, the regimes of high and low injection have no effect on J_{sc}. It is worth noting that J_{sc} is actually quite weakly dependent on carrier selectivity. As long as both carrier selectivities are greater than 100, the short circuit current will be greater than 98% of J_L. This should always be the case for solar cells that demonstrate an appreciable photovoltaic effect.

The V_{oc} can be calculated by setting J to zero and solving for V. This produces an identical expression to that which we derived in our previous work.[32] The expression, though complicated, can be greatly simplified when assuming the high and low injection limits. One can also numerically calculate the maximum power point using Eq. (12), and analytic expressions can be written down in the high and low injection limits. We will consider the case of both carriers in low injection and both carriers in high injection below, as they produce enlightening simplifications.

1. Low injection

If both carriers are in low injection, one can approximate the $J(V)$ (near the power quadrant) as

$$J(V) \approx \left(j_{0n}^{\alpha} + j_{0p}^{\beta}\right)e^{V/V_T} - J_L. \tag{18}$$

Note that this approximation requires the reasonable further assumption that the ratio of the j_0's is not large compared to both $\mathbf{J_0}$ and J_L ratios (see the supplementary material for details). This expression is remarkably simple; it is nearly identical to the $J(V)$ of the S-Q limit and the ideal solar cell [Eq. (1)]. The difference is simply that instead of $j_{0n}^{\alpha} + j_{0p}^{\beta}$, the S-Q limit contains a J_0 determined by radiative recombination. It is readily apparent from the form of Eq. (18) that in this regime, the superposition principle will apply, and the $J(V)$ will not be S-shaped around the power quadrant. One might note that Eq. (18) does not strictly go to zero when $V = 0$ and $J_L = 0$, which is simply a consequence of assuming that j_0's are negligibly small relative to J_L.

Importantly, the $J(V)$ curve in low injection is essentially independent of both $\mathbf{J_0}$'s. The recombination is quasi first-order and is dictated by the leakage of minority carriers at each contact. In low injection, one effectively assumes that both carrier selectivities are much greater than one, which means that $J_{sc} \approx J_L$. The V_{oc}, as derived in our previous work,[32] is given by

$$V_{oc} \approx V_T \ln\left(\frac{J_L}{j_{0n}^{\alpha} + j_{0p}^{\beta}}\right) \tag{19}$$

and is easily calculated from Eq. (18) by setting $J = 0$ and solving for V. The voltage at the maximum power point, V_m, is solved for in the usual fashion by finding the maximum of the power density function ($|J(V) \times V|$). In the low injection limit,

$$V_m \approx V_T\left(W\left[\frac{J_L e}{j_{0n}^{\alpha} + j_{0p}^{\beta}}\right] - 1\right). \tag{20}$$

The efficiency (given by $\eta = \frac{|J(V_m)\times V_m|}{P_{inc}}$, where P_{inc} is the incident power density) is solely determined by the ratio of J_L to $j_{0n}^{\alpha} + j_{0p}^{\beta}$. Again, Eq. (20) is identical to that derived in the S-Q limit except that J_0's are determined by the contacts instead of being set by radiative recombination. The comparison of the radiative J_0's to the contact-determined J_0's has already been considered in the literature; Swanson recognized that leakage at the contacts is the primary issue preventing silicon solar cells from approaching their optimal efficiency (after taking into account Auger recombination, reflection, and other unpreventable losses).[41]

2. High injection

When both carriers are in high injection, the $J(V)$ curve in the power quadrant can be approximated as

$$J(V) \approx J_L\left(\frac{1}{1+S_n e^{-V/V_T}} + \frac{1}{1+S_p e^{-V/V_T}} - 1\right), \tag{21}$$

where we have replaced the $\mathbf{J_0}/j_0$ ratios with the appropriate carrier selectivities (see the supplementary material for derivation). Both carrier selectivities must be much larger than one in order for J_{sc} to be equal to J_L. The light current linearly scales the "entire" curve, clearly violating superposition. The position of V_{oc} is independent of J_L. The approximation for V_{oc} was derived in our previous work

but can also easily be calculated by setting $J = 0$ in Eq. (21) and solving for V,

$$V_{oc} \approx V_T \ln\left(\sqrt{S_n S_p}\right). \tag{22}$$

Note that in high injection, the crossover voltage falls to its smallest possible value: V_{oc}. This is a consequence of linear scaling with J_L in high injection. In order to derive any analytic expression for the maximum power point in high injection, we must further assume that one carrier is limiting (i.e., we must assume that one carrier selectivity is much larger than the other). If we do so, the $J(V)$ behavior in the power quadrant is solely determined by said carrier, and the voltage at the maximum power point is equal to

$$V_m \approx V_T\left(W\left[\frac{S}{e}\right] + 1\right), \tag{23}$$

where S is the smaller (i.e., limiting) of the two carrier selectivities. As opposed to low injection, the V_m in high injection is independent of the light current and depends on both J_0's of the limiting carrier, similar to the V_{oc}. Unlike V_{oc}, however, the maximum power point is determined by the limiting carrier only, as long as the selectivities are significantly different. This is intuitive, given the nature of the $J(V)$ curve; the curve is nearly flat at V_{oc} in high injection, so the location of V_{oc} does not necessarily determine the efficiency because the fill factor can vary dramatically based on the location of the second step.

Assuming a J_L determined by 100% absorption above gap, one can readily compare the S-Q limiting efficiency (where J_0 is bandgap dependent) to the efficiency of our model in both the low and high injection limits with a fixed J_0 to get a picture of when contacts limit device behavior (as opposed to direct recombination). Refer to Figs. S3 and S4 in the supplementary material for quantitative comparisons assuming both low and high injection.

IV. SIMULATIONS

While the intention of the contact-determined theory is to provide an ideal limit to device behavior, we now proceed to demonstrate that our $J(V)$ theory can make accurate predictions about devices with physically relevant mobility and bulk recombination parameters. We nominally compare to simulations using a relatively high mobility of 1000 $\mathrm{cm^2\ V^{-1}\ s^{-1}}$, characteristic of single crystal absorbers, to focus on the contact-determined properties, but we also show deviations that occur as the mobility starts to limit the rate of collection/recombination at the contacts. We emphasize that the purpose of these simulations is not to show that our theory accurately describes all solar cells but to show that the assumptions we use do not prevent the theory from being relevant to a simple device with physical values for mobility and recombination and to show the utility of our model as a theoretical reference.

Simulations of $J(V)$ curves were performed by numerically solving the usual device physics equations in steady-state using the semiconductor module of COMSOL (see the supplementary material for details). We consider a generic undoped semiconducting absorber, whose bandgap is 1.5 eV and whose effective conduction and valence band densities of states are both $10^{19}\ \mathrm{cm^{-3}}$. Generation in the absorber followed a simple exponential (Beer–Lambert) position dependence, with an absorption coefficient of $3 \times 10^4\ \mathrm{cm^{-1}}$ so that 95% of the AM 1.5 spectrum above the bandgap is absorbed (see the supplementary material for details). Generation was neglected in the contacts for both architectures studied. Direct recombination, as determined by detailed balance consideration of the bandgap, and the absorption coefficient, was used throughout the absorber with a coefficient $B = 1.5 \times 10^{-11}\ \mathrm{cm^3\ s^{-1}}$. Shockley–Read–Hall recombination and Auger recombination were neglected. The absorber was contacted with either Schottky metal contacts or wide-gap doped semiconductors to test the utility of the theory with various architectures.

A. Schottky contacts

Schottky metal contacts (denoted the α and β contacts) were set as the boundary conditions for the partial currents on either side of the absorber, which was 1 μm thick. The corresponding J_0's are

$$\mathbf{J_{0n}^{\beta}} = \mathbf{J_{0p}^{\alpha}} = A^* T^2 e^{-\frac{E_g - \Delta\phi}{2qV_T}}, \tag{24a}$$

$$j_{0p}^{\beta} = j_{0n}^{\alpha} = A^* T^2 e^{-\frac{E_g + \Delta\phi}{2qV_T}}, \tag{24b}$$

where A^* is the Richardson constant and the parameter $\Delta\phi$ is a measure of how far the two contacts' work functions are separated in volts. The contact work functions are equidistant from the intrinsic Fermi level of the absorber so that with, for instance, $\Delta\phi = 0.2$ V, the work function of contact α is 0.1 eV below the intrinsic level and vice versa for the β contact. In general, there could be four different effective A^*'s. For simplicity, we have assumed that all four are equal. Refer to the supplementary material for a table collecting all parameters set in the simulation.

Figure 5 compares the simulated vs theoretical $J(V)$ curves of a device with selective Schottky diodes used for each contact. A^* was

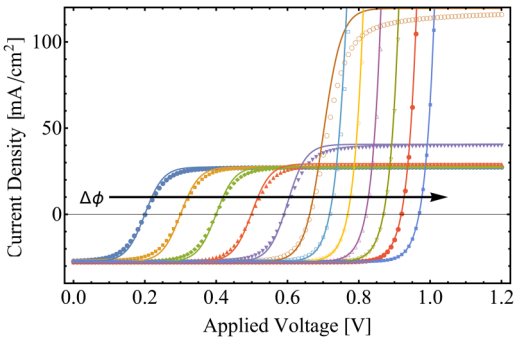

FIG. 5. Plot of $J(V)$ comparing simulations (data points) to Eq. (12) (solid lines) for a 1.5 eV bandgap intrinsic absorber with Schottky metal contacts with varying work functions as determined by $\Delta\phi$. The $\Delta\phi$ increases from 0.2 to 1.3 eV in steps of 0.1 and $A^* = 3\ \mathrm{A\,cm^{-2}\,K^{-2}}$. Note that because all A^*'s are the same, the electron and hole steps line up on top of each other so that the size of the step is twice as large as a single step.

set to 3 A cm^{-2} K^{-2}, within the wide range of reported Richardson constants for thin-film semiconductors.[42–45] At low $\Delta\phi$, both electrons and holes are in high injection. Because the two j_0's are equal as well as the two $\mathbf{J_0}$'s, both the electron and hole steps are on top of each other, we can only see one step. The size of the step is approximately $2J_L$ as long as the $\mathbf{J_0}$ is much smaller than J_L. As the $\mathbf{J_0}$ becomes comparable to J_L at $\Delta\phi = 0.6$ eV, the $J(V)$ curve transitions to low injection, and the step size becomes larger than $2J_L$.

The V_{oc}'s as predicted by the theory are accurate for every $\Delta\phi$ shown. However, for many of the $\Delta\phi$ values, the theoretical limit has a slightly larger fill factor than the simulated data. For the lower $\Delta\phi$ values, the fill factor is reduced in the simulated data because the mobility limits current collection when the carrier densities are low. At higher $\Delta\phi$, the higher carrier selectivities can support higher voltages and thus larger carrier densities in the bulk. The larger carrier densities in the bulk allow for higher conductivities, thus reducing the need for high mobility and, therefore, the fill factor deficit is reduced. Using increased bulk recombination does limit the V_{oc}'s for the largest values of $\Delta\phi$ (see the supplementary material).

We expect that the addition of Auger recombination (or any other form of bulk recombination) to the simulation would decrease the V_{oc}'s and hence, the efficiency, further from the contact-determined values for high $\Delta\phi$'s, while it should not affect the performance for lower values of $\Delta\phi$. This is because bulk recombination only serves as a limitation when the carrier selectivities are very large. This effect would become more pronounced with light intensities over one sun.

Figure 6 compares the theoretical efficiency [calculated numerically from Eq. (12)] of the device under discussion to the simulated efficiencies for various light intensities. The number of suns Φ_L was varied exponentially from 10^{-3} to 10^2. The region where the lines converge denotes high injection, and each different light intensity curve moves off of the high injection curve at different values of $\Delta\phi$, as expected from our definitions of high and low injection. Whereas in high injection, the efficiency is independent of light intensity, in low injection, the efficiency becomes quasilogarithmically dependent on light intensity as we expect from Eq. (20). The simulated efficiencies in high injection are slightly below the theoretical limit due to finite mobility, as discussed above. At high $\Delta\phi$, the theory provides accurate predictions when using bulk recombination set by the radiative limit, as we have here. Again, increased bulk recombination does have a small effect on the efficiencies for the highest $\Delta\phi$'s (see the supplementary material).

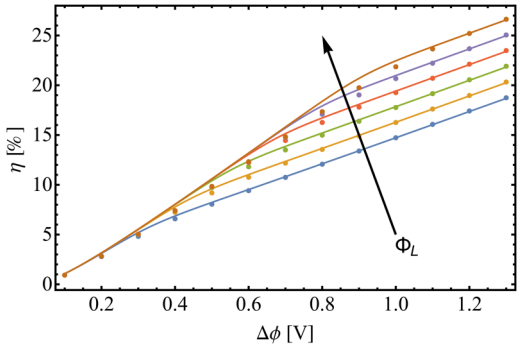

FIG. 6. Simulated efficiency (data points) compared to that derived from Eq. (12) (solid lines) for the same device as Fig. 5 with $A^* = 3$ A cm^{-2} K^{-2} and $\Delta\phi$ increasing from 0.1 to 1.3 eV in steps of 0.1. The number of suns, Φ_L, was exponentially varied from 10^{-3} to 10^2 by factors of 10.

Our theoretical model works well, then, for a generic device with Schottky contacts as long as the mobility does not limit the rate at which carriers escape to the contacts. Of course, the model is expected to become less accurate as the mobility is decreased, or equivalently as J_0's become larger with a fixed mobility (i.e., when bulk transport starts to limit the speed at which carriers can recombine at the contacts). This is indeed the case as can be seen in Fig. 7(a) where the Richardson constant is varied from 10^{-2} A cm^{-2} K^{-2} to its ideal metal limit (~ 100 A cm^{-2} K^{-2}), with a fixed $\Delta\phi = 1.0$ eV. The model becomes less accurate as A^* approaches 100 A cm^{-2} K^{-2}. Specifically, the fill factor and J_{sc} are poor relative to the theory; however, the V_{oc} is actually larger than the theory predicts. This concept has been discussed extensively in the literature[19,46–49] and the higher V_{oc}'s were further demonstrated in our previous work.[32] Put simply, when the mobility is reduced to the point where carriers generated in the bulk cannot reach the contacts as fast as they recombine at the contacts, the actual contact recombination rate is smaller than that predicted by J_0's, leading to a larger-than-predicted V_{oc}. However, the limited mobility also reduces the fill factor and J_{sc} as previously discussed. It is possible for the J_{sc} as well as V_{oc} to be improved by poor carrier mobility, though this occurs with very poor contacts and/or very low light intensities.

Similar deviations from the theory occur in Fig. 7(b), where the A^* is varied over the same range, but the asymmetry is reduced ($\Delta\phi = 0.5$ eV). The deviation is much more evident outside of the power quadrant for the largest A^* and is expected given that the limited asymmetry/selectivity prevents large quasi-Fermi-level splitting, limiting the carrier density and thus the conductivity in the bulk.

B. *p-i-n* heterostructure

For comparison, we have included simulations of a *p-i-n* structure with the absorber described above, where the contacts are wider bandgap, doped semiconductors. This structure bears resemblance to a large number of thin-film technologies, where an intrinsic or lightly doped absorber is sandwiched by two thin, sometimes entirely different, semiconductors with opposite doping type. In the simulation, the absorber is sandwiched by equally doped *n* and *p* doped semiconductors with bandgaps 1.7 and 1.9 eV on either side (see Fig. 8). The absorber/contact interface is simulated with thermionic emission boundary conditions. The wide-bandgap contacts are, in turn, contacted by ohmic metal contacts. To vary the selectivity in a similar manner as before, the doping density of each contact is varied over a wide range of values. Note that there is no reason why the dopant densities have to be equal; this choice is made for the sake of simplicity.

We calculate the effective J_0's for such a structure by using a barrier height for either contact as set by the energy difference

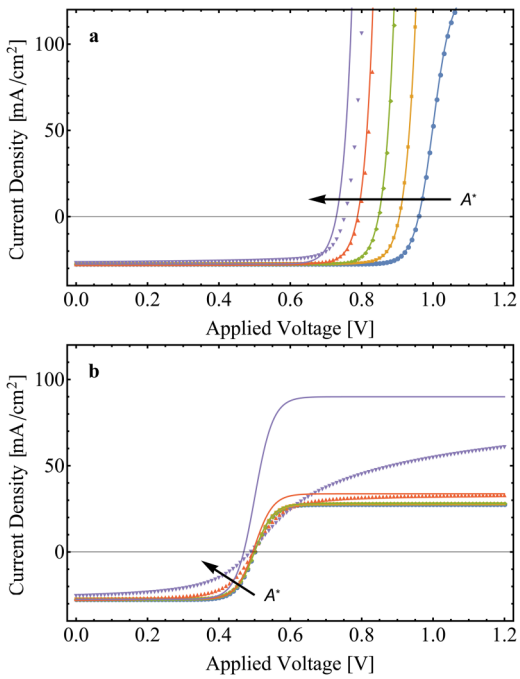

FIG. 7. Simulated $J(V)$ (data points) compared with the theory (lines) for a semiconductor ($E_g = 1.5\,\text{eV}$) and Schottky metal contacts with metal work functions set b: (a) $\Delta\phi = 1.0\,\text{eV}$ and (b) 0.5 eV. In both cases, A^* was increased from 10^{-2} to $10^2\,\text{A cm}^{-2}\,\text{K}^{-2}$ by factors of 10. Note that in (b), the curves with lower A^* lie on top of each other, because in high injection, the $J(V)$ curve is only dependent on the selectivity, not the magnitudes of J_0's.

between the Fermi level and the appropriate band edge (see Fig. 8). Thus, we are essentially treating thin doped semiconductors as Schottky contacts. This is only expected to work as long as the Fermi levels of the contacts (as set by the dopant density) remain within the bandgap of the absorber. We expect that for thicker doped contacts, diffusion, rather than thermionic emission will be the rate limiting process for the partial currents, and thus J_0's for the contacts would be governed by the Shockley model. See Fig. S6 in the supplementary material for simulations detailing the transition between the two regimes.

The effective A^* is calculated according to

$$A^* = A_h^* = A_e^* = \frac{4\pi m^* k_B^2 q}{h^3}, \tag{25}$$

where h is Planck's constant, and m^* is the carrier effective mass, given by

$$m^* = m_h^* = m_e^* = \frac{h^2}{2\pi k_B T}\left(\frac{N_c}{2}\right)^{2/3}. \tag{26}$$

The effective masses and thus A^*'s are equal because we have assumed that $N_c = N_v$. Given a value of $1 \times 10^{19}\,\text{cm}^{-3}$ for each of the effective densities of states, both effective A^*'s are equal to $65\,\text{A cm}^{-2}\,\text{K}^{-2}$.

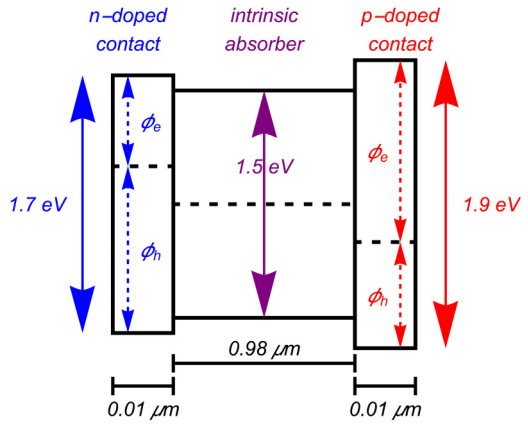

FIG. 8. Schematic depicting the device structure (before equilibrating) used for the *p-i-n* simulations. Note that the *x*-axis is not to scale. Fermi levels for each layer are indicated by the dashed lines; the contact Fermi levels are determined by the doping density, which is varied in the simulation by orders of magnitude. The electron affinity of each layer is set so that the intrinsic layers of each semiconductor are aligned and that the offsets of both bands at a given interface are equal. The effective barrier heights used to calculate each of the four J_0's are indicated by the dashed red and blue arrows. The Fermi level (dashed line) of the n contact is set by $E_c - E_f = k_B T \ln\left(\frac{N_c}{N_d}\right)$, while the $E_f - E_v = k_B T \ln\left(\frac{N_v}{N_d}\right)$ sets the Fermi level of the p contact.

Figure 9(a) compares simulated $J(V)$ curves for the *p-i-n* heterostructure to those calculated with Eq. (12) with A^*'s given by Eq. (25) and barrier heights set by the blue and red ϕ_e's and ϕ_h's from Fig. 8. The dopant density of each contact, N_d is varied in unison from 10^7 to $10^{15}\,\text{cm}^{-3}$ to produce the different curves. Two steps are observed in most of the curves, because although the A^*'s on each side are identical, the effective barrier heights are not, leading to different selectivities for electrons and holes. The transition from low to high injection occurs around $N_d = 10^{11}\,\text{cm}^{-3}$, meaning most practical devices of this type would operate in low injection under one sun. While the theory does not exactly match the simulation for voltages beyond V_{oc}, it is quite accurate inside of the power quadrant.

Finally, Fig. 9(b) compares the *p-i-n* heterojunction simulations with the theory for a fixed $N_d = 10^{12}\,\text{cm}^{-3}$ for both contacts while the generation rate is varied. Therefore, J_0's are fixed, while only J_L varies. The model is able to reproduce both steps, as well as the transition from low to high injection, which occurs around 10 suns in this case. The dopant density of the contacts is quite low here; for higher dopant densities, it requires unrealistically high generation rates to push the device into high injection. With an absorber whose bandgap is 1.5 eV, it is clear that most practical dopant densities will result in the device working in low injection, at which point the device will be limited by recombination, as opposed to selectivity/asymmetry. This is not surprising; doped heterojunction and homojunction contacts are among the most effective contact technologies as long as an ohmic contact can be made to the doped semiconductors.

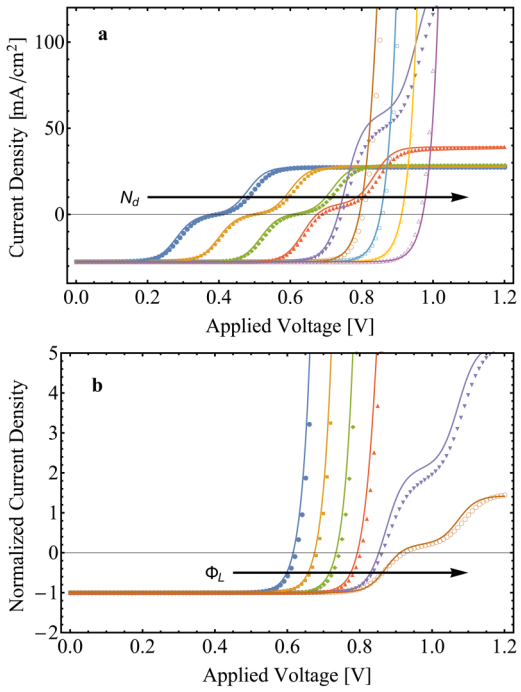

FIG. 9. Simulated $J(V)$ curves (data points) compared with Eq. (12) (lines) for the *p-i-n* heterostructure. In (a), the dopant density N_d of both contacts is simultaneously stepped from 10^7 to 10^{15} cm^{-3}, by factors of 10. For (b), the dopant densities of the contacts are fixed at 10^{12} cm^{-3}, the number of suns Φ_L is varied from 10^{-3} to 10^2 by factors of ten, and the current density is normalized by the short circuit current for each different light intensity.

V. CONCLUSION

We have presented a straightforward analytic model describing the $J(V)$ curve of a contact-limited solar cell determined by the four equilibrium exchange current densities of both electrons and holes for each contact. Unlike numerical models, our model provides clear quantitative relations between the observed $J(V)$ features and their fundamental cause, as quantified by the four values of the exchange current densities. The contact-determined $J(V)$ curve consists of two smeared-out step functions, offset approximately by J_L, the current due to illumination. The voltages at which the steps occur are determined by the carrier selectivities [as defined in Eq. (14)] of electron and hole J_0's separately. The goal of making an efficient solar cell in this case amounts to pushing the first step as far out into forward bias as possible, thus a large carrier selectivity for "both" carriers is required in an efficient solar cell.

The shape of the $J(V)$ curve in the power quadrant is determined by the relation of the limiting $\mathbf{J_0}$ to J_L, delineating the high and low injection regimes as defined in Sec. III. In low injection, the $J(V)$ curve looks ideal, and the cell's performance is primarily limited by quasi-first-order contact recombination caused by leakage of the limiting carrier, as determined by the appropriate j_0. In high injection (unless both carrier selectivities are equal), the $J(V)$ curve is S-shaped in the power quadrant and levels off at $J \approx 0$, leading to a lower fill factor and an efficiency determined by the selectivity of the limiting carrier. It is clear that the nonideal behaviors such as S-shaped curves and failure of current superposition are consequences of the finite extraction rate of majority carriers at their contacts, thus comparison of J_L to the $\mathbf{J_0}$'s will determine whether or not a contact-limited solar cell should display such behavior within sight of the power quadrant. Additionally, when the $J(V)$ curve is in high injection and is S-shaped, the device can be improved not only by increasing the extraction rate of the relevant majority carrier as is often understood but also by reducing the leakage rate of said carrier at the opposite contact.

Simulated $J(V)$ curves are presented to establish that the analytic model is quantitatively accurate for a 1D device with Schottky metal contacts, as well as a 1D *p-i-n* heterostructure. The model may potentially be extended to more complicated structures; however, care must be taken to determine whether the effective J_0 set by those structures is truly voltage independent. The goal of the model, like that of the S-Q limit, is to provide an ideal limit of device performance as determined by measurable device properties. While it is possible to exceed this limit if the mobility is low enough to limit the speed of contact recombination, this is not expected for devices with reasonably selective contacts and good mobilities.

Comparison to the S-Q limit allows determination of the necessary contact properties required to approach the radiative recombination limit. Additionally, the shape of the $J(V)$ curve is indicative of what needs to be improved in order to increase device efficiency; an S-shape indicates that appropriate improvements in "either" contact will improve efficiency, while an ideal looking $J(V)$ curve that is contact-limited indicates protection from leakage of the limiting minority process is the only way to improve device performance. Our model will be particularly useful to scientists studying relatively new absorbers whose contacts have yet to be fully optimized.

SUPPLEMENTARY MATERIAL

See the supplementary material for the algebraic derivation of the $J(V)$ curve and limiting cases, the physical explanation of the $J(V)$ curve, simulation details, and simulations assessing how one can measure the four J_0's of the two interfaces needed to make a solar cell.

ACKNOWLEDGMENTS

This work was funded by the Division of Chemical Sciences, Geosciences, and Biosciences, Office of Basic Energy Sciences of the U.S. Department of Energy through Grant No. DE-SC0012363.

REFERENCES

[1]W. Shockley and H. J. Queisser, "Detailed balance limit of efficiency of p-n junction solar cells," J. Appl. Phys. **32**, 510–519 (1961).
[2]W. Ruppel and P. Würfel, "Upper limit for the conversion of solar energy," IEEE Trans. Electron Devices **27**, 877–882 (1980).
[3]A. De Vos, "Detailed balance limit of the efficiency of tandem solar cells," J. Phys. D Appl. Phys **13**, 839 (1980).
[4]H. Pauwels and A. D. Vos, "Determination of the maximum efficiency solar cell structure," Solid-State Electron. **24**, 835–843 (1981).

[5]T. Tiedje, E. Yablonovitch, G. Cody, and B. Brooks, "Limiting efficiency of silicon solar cells," IEEE Trans. Electron Devices **31**, 711–716 (1984).
[6]P. Würfel, *Physics of Solar Cells: From Basic Principles to Advanced Concepts*, 2nd ed. (Wiley-VCH, Weinheim, 2009).
[7]E. L. Ratcliff, B. Zacher, and N. R. Armstrong, "Selective interlayers and contacts in organic photovoltaic cells," J. Phys. Chem. Lett. **2**, 1337–1350 (2011).
[8]R. Po, C. Carbonera, A. Bernardi, and N. Camaioni, "The role of buffer layers in polymer solar cells," Energy Environ. Sci. **4**, 285–310 (2011).
[9]F. Feldmann, M. Simon, M. Bivour, C. Reichel, M. Hermle, and S. W. Glunz, "Carrier-selective contacts for Si solar cells," Appl. Phys. Lett. **104**, 181105 (2014).
[10]E. J. Juarez-Perez, M. Wußler, F. Fabregat-Santiago, K. Lakus-Wollny, E. Mankel, T. Mayer, W. Jaegermann, and I. Mora-Sero, "Role of the selective contacts in the performance of lead halide perovskite solar cells," J. Phys. Chem. Lett. **5**, 680–685 (2014).
[11]S. Wheeler, F. Deledalle, N. Tokmoldin, T. Kirchartz, J. Nelson, and J. R. Durrant, "Influence of surface recombination on charge-carrier kinetics in organic bulk heterojunction solar cells with nickel oxide interlayers," Phys. Rev. Appl. **4**, 024020 (2015).
[12]C. Battaglia, S. M. De Nicolas, S. De Wolf, X. Yin, M. Zheng, C. Ballif, and A. Javey, "Silicon heterojunction solar cell with passivated hole selective MoOx contact," Appl. Phys. Lett. **104**, 113902 (2014).
[13]C. Reichel, U. Würfel, K. Winkler, H.-F. Schleiermacher, M. Kohlstädt, M. Unmüssig, C. A. Messmer, M. Hermle, and S. W. Glunz, "Electron-selective contacts via ultra-thin organic interface dipoles for silicon organic heterojunction solar cells," J. Appl. Phys. **123**, 024505 (2018).
[14]X. Yang, E. Aydin, H. Xu, J. Kang, M. Hedhili, W. Liu, Y. Wan, J. Peng, C. Samundsett, A. Cuevas *et al.*, "Tantalum nitride electron-selective contact for crystalline silicon solar cells," Adv. Energy Mater. **8**, 1800608 (2018).
[15]A. Niemegeers and M. Burgelman, "Effects of the Au/CdTe back contact on IV and CV characteristics of Au/CdTe/CdS/TCO solar cells," J. Appl. Phys. **81**, 2881–2886 (1997).
[16]A. Wagenpfahl, D. Rauh, M. Binder, C. Deibel, and V. Dyakonov, "S-shaped current-voltage characteristics of organic solar devices," Phys. Rev. B **82**, 115306 (2010).
[17]O. J. Sandberg, M. Nyman, and R. Österbacka, "Effect of contacts in organic bulk heterojunction solar cells," Phys. Rev. Appl. **1**, 024003 (2014).
[18]R. Brendel and R. Peibst, "Contact selectivity and efficiency in crystalline silicon photovoltaics," IEEE J. Photovolt. **6**, 1413–1420 (2016).
[19]O. J. Sandberg, A. Sundqvist, M. Nyman, and R. Österbacka, "Relating charge transport, contact properties, and recombination to open-circuit voltage in sandwich-type thin-film solar cells," Phys. Rev. Appl. **5**, 044005 (2016).
[20]S. Solak, A. G. Ricciardulli, T. Lenz, N. I. Crăciun, P. W. M. Blom, and G. A. H. Wetzelaer, "Open-circuit voltage loss in annealed P3HT:Perylene diimide bulk heterojunction solar cells," Appl. Phys. Lett. **110**, 163301 (2017).
[21]R. V. K. Chavali, J. R. Wilcox, B. Ray, J. L. Gray, and M. A. Alam, "Correlated nonideal effects of dark and light I–V characteristics in a-Si/c-Si heterojunction solar cells," IEEE J. Photovolt. **4**, 763–771 (2014).
[22]U. Das, S. Hegedus, L. Zhang, J. Appel, J. Rand, and R. Birkmire, "Investigation of hetero-interface and junction properties in silicon heterojunction solar cells," in *Proceedings of 35th IEEE Photovoltaic Specialists Conference* (IEEE, 2010), pp. 001358–001362.
[23]I. Mora-Sero and J. Bisquert, "Effect of reduced selectivity of contacts on the current-potential characteristics and conversion performance of solar cells," Sol. Energ. Mater. Sol. Cells **85**, 51–62 (2004).
[24]C. Crowell and S. Sze, "Current transport in metal-semiconductor barriers," Solid-State Electron. **9**, 1035–1048 (1966).
[25]R. E. Brandt, N. M. Mangan, J. V. Li, Y. S. Lee, and T. Buonassisi, "Determining interface properties limiting open-circuit voltage in heterojunction solar cells," J. Appl. Phys. **121**, 185301 (2017).
[26]S. M. Sze and M. K. Lee, *Semiconductor Devices, Physics and Technology*, 3rd ed. (Wiley, Hoboken, NJ, 2012).
[27]W. Shockley, "The theory of p-n junctions in semiconductors and p-n junction transistors," Bell Syst. Tech. J **28**, 435–489 (1949).
[28]E. Yablonovitch, T. Gmitter, R. M. Swanson, and Y. H. Kwark, "A 720 mv open circuit voltage SiOx:c-Si:SiOx double heterostructure solar cell," Appl. Phys. Lett. **47**, 1211–1213 (1985).
[29]T. Mikio, T. Akira, M. Eiji, and T. Makoto, "Obtaining a higher Voc in HIT cells," Prog. Photovolt. Res. Appl. **13**, 481–488 (2005).
[30]K. Yoshikawa, H. Kawasaki, W. Yoshida, T. Irie, K. Konishi, K. Nakano, T. Uto, D. Adachi, M. Kanematsu, H. Uzu *et al.*, "Silicon heterojunction solar cell with interdigitated back contacts for a photoconversion efficiency over 26%," Nat. Energy **2**, 17032 (2017).
[31]R. M. Swanson, "Back side contact solar cell with doped polysilicon regions," U.S. patent 7,468,485 (Dec. 23, 2008).
[32]E. T. Roe, K. E. Egelhofer, and M. C. Lonergan, "Limits of contact selectivity/recombination on the open-circuit voltage of a photovoltaic," ACS Appl. Energy Mater. **1**, 1037–1046 (2018).
[33]E. H. Rhoderick and R. H. Williams, *Metal-Semiconductor Contacts* (Clarendon Press, New York, 1988).
[34]M. X. Tan, P. E. Laibinis, S. T. Nguyen, J. M. Kesselman, C. E. Stanton, and N. S. Lewis, "Principles and applications of semiconductor photoelectrochemistry," Prog. Inorg. Chem. **41**, 21–144 (1994).
[35]S. M. Sze, *Modern Semiconductor Device Physics* (Wiley, New York, 1998).
[36]F. E. Jones, C. Daniels-Hafer, B. P. Wood, R. G. Danner, and M. C. Lonergan, "Current transport at the p-InP—poly(pyrrole) interface," J. Appl. Phys. **90**, 1001–1010 (2001).
[37]C. Daniels-Hafer, M. Jang, S. W. Boettcher, R. G. Danner, and M. C. Lonergan, "Tuning charge transport at the interface between indium phosphide and a polypyrrole-phosphomolybdate hybrid through manipulation of electrochemical potential," J. Phys. Chem. B **106**, 1622–1636 (2002).
[38]F. A. Lindholm, J. G. Fossum, and E. L. Burgess, "Application of the superposition principle to solar-cell analysis," IEEE Trans. Electron Devices **26**, 165–171 (1979).
[39]J. E. Moore, S. Dongaonkar, R. V. K. Chavali, M. A. Alam, and M. S. Lundstrom, "Correlation of built-in potential and I–V crossover in thin-film solar cells," IEEE J. Photovolt. **4**, 1138–1148 (2014).
[40]J. Pan, M. Gloeckler, and J. R. Sites, "Hole current impedance and electron current enhancement by back-contact barriers in CdTe thin film solar cells," J. Appl. Phys. **100**, 124505 (2006).
[41]R. M. Swanson, "Approaching the 29% limit efficiency of silicon solar cells," in *2005 Conference Record of the Thirty-First IEEE Photovoltaic Specialists Conference* (Jan 3, 2005), pp. 889–894.
[42]A. Srivastava, B. Arora, and S. Guha, "Measurement of Richardson constant of GaAs schottky barriers," Solid-State Electron. **24**, 185–191 (1981).
[43]M. Missous, E. H. Rhoderick, D. A. Woolf, and S. P. Wilkes, "On the Richardson constant of intimate metal-GaAs schottky barriers," Semicond. Sci. Technol. **7**, 218–221 (1992).
[44]M. Pattabi, S. Krishnan, Ganesh, and X. Mathew, "Effect of temperature and electron irradiation on the I–V characteristics of Au/CdTe schottky diodes," Solar Energy **81**, 111–116 (2007).
[45]J. Ge, J. Chu, J. Jiang, Y. Yan, and P. Yang, "Characteristics of In-substituted CZTS thin film and bifacial solar cell," ACS Appl. Mater. Interfaces **6**, 21118–21130 (2014).
[46]C. Deibel, A. Wagenpfahl, and V. Dyakonov, "Influence of charge carrier mobility on the performance of organic solar cells," Phys. Status Solidi Rapid Res. Lett. **2**, 175–177 (2008).
[47]T. Kirchartz, B. E. Pieters, K. Taretto, and U. Rau, "Mobility dependent efficiencies of organic bulk heterojunction solar cells: Surface recombination and charge transfer state distribution," Phys. Rev. B **80**, 035334 (2009).
[48]W. Tress, K. Leo, and M. Riede, "Optimum mobility, contact properties, and open-circuit voltage of organic solar cells: A drift-diffusion simulation study," Phys. Rev. B **85**, 155201 (2012).
[49]A. Spies, M. List, T. Sarkar, and U. Würfel, "On the impact of contact selectivity and charge transport on the open-circuit voltage of organic solar cells," Adv. Energy Mater. **7**, 1601750 (2017).